PERGAMON

International Journal of Solids and Structures 38 (2001) 3281–3299

INTERNATIONAL JOURNAL OF SOLIDS and STRUCTURES

www.elsevier.com/locate/ijsolstr

Modal control of smart shells by optimized discretely distributed piezoelectric transducers

Dongchang Sun [a,b], Liyong Tong [a,*]

[a] *Department of Aeronautical Engineering, University of Sydney, Building J07, Sydney, NSW 2006, Australia*
[b] *School of Mechanical Engineering, Hebei University of Technology, Tianjin 300130, People's Republic of China*

Received 12 December 1999; in revised form 1 May 2000

Abstract

Active vibration control of the shell structures with discretely distributed piezoelectric sensor and actuator patches is investigated. The quasi-modal sensor is developed to estimate the dominant mode coordinates of the shell from the outputs of the sensor patches, and a criterion for finding the optimal locations and sizes of the sensor elements is given by minimizing the observation spillover. The quasi-modal actuator is also designed to actuate the designated modes by means of modulating the voltage distribution of the piezoelectric actuator patches, and a criterion for optimal placement of the actuator patches is presented based on the energy and control spillover consideration. Furthermore, the compensators are employed to filter out the residual components with high frequencies from the estimated modal coordinates. Based on the quasi-modal sensor and quasi-modal actuator, the independent modal control is performed approximately to control the vibration of smart shells. The simulation examples show that the vibration of the shells can be controlled effectively by using the presented method.

Keywords: Vibration damping; Shells; Piezoelectric transducers; Modal control; Optimization

1. Introduction

The smart shell structures with integrated piezoelectric sensor and actuator laminae have been widely investigated in the past decade. The research work mainly focuses on modelling, finite element formulation and vibration control of the smart shells (Tzou and Gadre, 1989; Tzou, 1992; Thrupathi and Naganathan, 1993; Koconis et al., 1994; Tzou et al., 1994; Saravanos, 1996; Miller and Abramovich, 1996; Pletner and Abramovich, 1997; Chandrashekhara et al., 1998; Henry and Clark, 1999). Chee et al. (1998) gave an detailed review on the modelling of the piezoelectric intelligent structures. Based on the mathematical models, several simple control laws such as proportional and derivative (PD) method and Liapunov method are used in active vibration control of the smart shells (Tzou, 1992). Moreover, the independent

* Corresponding author. Tel.: +61-2-351-6949; fax: +61-2-351-4841.
E-mail address: ltong@aero.usyd.edu.au (L. Tong).

0020-7683/01/$ - see front matter
PII: S0020-7683(00)00224-9

modal space control method, which cannot be realized satisfactorily by the traditional discrete sensors and actuators, can be implemented by using the modal sensor/actuator designed by the distributed piezoelectric sensor and actuator laminae.

Compared to the modelling and the finite-element method (FEM) formulating of smart shells, less control schemes are developed for vibration control of smart shells. Although modal sensor and actuator (Lee and Moon, 1990; Tzou et al., 1994) can be designed by shaping the electrode patterns of the piezoelectric laminae in one dimensional case such as ring, it is difficult, if not impossible, to be applied in the general smart shell structures. Despite some control schemes developed for smart beams and plates (Sun et al., 1997, 1999a,b), which needs the fully covered piezoelectric sensor and actuator laminae, can be generalized to shell case, it is impractical that the whole structure is covered completely by the piezoelectric sensor and actuator layers for large shell structures. A reasonable method may be that several discretely distributed piezoelectric patches, each of which only covers a local area on the host shell, are properly located and used as the sensor and actuator patches to perform its vibration control.

In this paper, vibration control of the thin smart shell structures with attached discretely distributed piezoelectric sensor and actuator wafers is investigated. Quasi-modal sensor is designed to estimate the first several dominant modal coordinates approximately from the output voltages of the sensor wafers. Moreover, a compensator for each mode to be controlled is used to suppress the observation spillover and maintain stability of the closed-loop system. Also, the quasi-modal actuator is designed to generate the desired modal forces for the designated modes by applying proper voltage distribution on actuator wafers. Based on the quasi-modal sensor and actuator, the quasi-independent modal control of the shell structures can be performed. The criteria for finding the optimal locations and sizes of the piezoelectric sensor and actuator patches are given respectively based on spillover and energy considerations. Finally, simulation examples are given to demonstrate the effectiveness of the present method.

2. Sensor and actuator equations for smart shell

Consider a thin elastic shell on which several piezoelectric patches are bonded as the distributed sensor and actuator respectively, as shown in Fig. 1. The tri-orthogonal curvilinear coordinate system with axes α_1, α_2 and α_3, is also schematically shown in Fig. 1. The two Lame parameters for α_1 and α_2 axes are A_1 and A_2, and the radii of curvature are R_1 and R_2, respectively. Assume that the piezoelectric patches are much thinner than the host shell, and the composite smart shell is still thin. The piezoelectric patches are assumed to be bonded perfectly on the host shell and the effects of the bonding material on the properties of the whole shell are neglected.

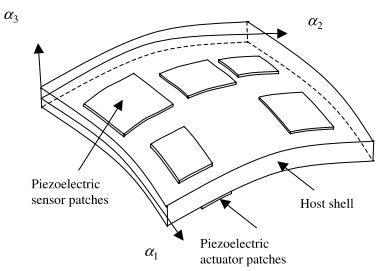

Fig. 1. The smart shell with discretely distributed piezoelectric transducers.

For the case that the shell is fully covered by the sensor and actuator laminae, the output voltage generated by the piezoelectric sensor lamina due to the strain of the shell can be derived as (Tzou, 1992)

$$V^{s} = -\frac{h_s}{\epsilon_{33} S^{e}} \int\int_{S^{e}} \left\{ \left[e_{31} \left(\frac{1}{A_1} \frac{\partial u_1}{\partial \alpha_1} + \frac{u_2}{A_1 A_2} \frac{\partial A_1}{\partial \alpha_2} + \frac{u_3}{R_1} \right) + e_{32} \left(\frac{1}{A_2} \frac{\partial u_2}{\partial \alpha_2} + \frac{u_1}{A_1 A_2} \frac{\partial A_2}{\partial \alpha_1} + \frac{u_3}{R_2} \right) \right] \right.$$
$$+ e_{31} r_1^{s} \left[\frac{1}{A_1} \frac{\partial}{\partial \alpha_1} \left(\frac{u_1}{R_1} - \frac{1}{A_1} \frac{\partial u_3}{\partial \alpha_1} \right) + \frac{1}{A_1 A_2} \left(\frac{u_2}{R_2} - \frac{1}{A_2} \frac{\partial u_3}{\partial \alpha_2} \right) \frac{\partial A_1}{\partial \alpha_2} \right]$$
$$\left. + e_{32} r_2^{s} \left[\frac{1}{A_2} \frac{\partial}{\partial \alpha_2} \left(\frac{u_2}{R_2} - \frac{1}{A_2} \frac{\partial u_3}{\partial \alpha_2} \right) + \frac{1}{A_1 A_2} \left(\frac{u_1}{R_1} - \frac{1}{A_1} \frac{\partial u_3}{\partial \alpha_1} \right) \frac{\partial A_2}{\partial \alpha_1} \right] \right\} A_1 A_2 \, \mathrm{d}\alpha_1 \, \mathrm{d}\alpha_2, \tag{1}$$

where u_1, u_2 and u_3 are the displacements of the neutral surface in three directions; e_{31} and e_{32}, the piezoelectric stress constants of the sensor layer; ϵ_{33}, the dielectric constant of the sensor; S^{e}, the effective area of the sensor layer; h_s, the thickness of the sensor, and r_1^{s} and r_2^{s} are the z coordinates of the mid-surface of the sensor lamina from the neutral surface of the shell.

The differential equations of motion of the smart shell can be expressed as

$$-\frac{\partial (N_{11} A_2)}{\partial \alpha_1} - \frac{\partial (N_{21} A_1)}{\partial \alpha_2} - N_{12} \frac{\partial A_1}{\partial \alpha_2} + N_{22} \frac{\partial A_2}{\partial \alpha_1}$$
$$- \frac{1}{R_1} \left[\frac{\partial (M_{11} A_2)}{\partial \alpha_1} + \frac{\partial (M_{21} A_1)}{\partial \alpha_2} + M_{12} \frac{\partial A_1}{\partial \alpha_2} - M_{22} \frac{\partial A_2}{\partial \alpha_1} \right] + A_1 A_2 \rho h \ddot{u}_1 = A_1 A_2 F_1^{a}$$
$$-\frac{\partial (N_{12} A_2)}{\partial \alpha_1} - \frac{\partial (N_{22} A_1)}{\partial \alpha_2} - N_{21} \frac{\partial A_2}{\partial \alpha_1} + N_{11} \frac{\partial A_1}{\partial \alpha_2}$$
$$- \frac{1}{R_2} \left[\frac{\partial (M_{12} A_2)}{\partial \alpha_1} + \frac{\partial (M_{22} A_1)}{\partial \alpha_2} + M_{21} \frac{\partial A_2}{\partial \alpha_1} - M_{11} \frac{\partial A_1}{\partial \alpha_2} \right] + A_1 A_2 \rho h \ddot{u}_2 = A_1 A_2 F_2^{a} \tag{2}$$
$$-\frac{\partial}{\partial \alpha_1} \left\{ \frac{1}{A_1} \left[\frac{\partial (M_{11} A_2)}{\partial \alpha_1} + \frac{\partial (M_{21} A_1)}{\partial \alpha_2} + M_{12} \frac{\partial A_1}{\partial \alpha_2} - M_{22} \frac{\partial A_2}{\partial \alpha_1} \right] \right\}$$
$$- \frac{\partial}{\partial \alpha_2} \left\{ \frac{1}{A_2} \left[\frac{\partial (M_{12} A_2)}{\partial \alpha_1} + \frac{\partial (M_{22} A_1)}{\partial \alpha_2} + M_{21} \frac{\partial A_2}{\partial \alpha_1} - M_{11} \frac{\partial A_1}{\partial \alpha_2} \right] \right\}$$
$$+ A_1 A_2 \left(\frac{N_{11}}{R_1} + \frac{N_{22}}{R_2} \right) + A_1 A_2 \rho h \ddot{u}_3 = A_1 A_2 F_3^{a},$$

where ρ and h are the mass density and the thickness of the shell, respectively, and the membrane forces N_{11}, N_{22}, N_{12} as well as the bending moments M_{11}, M_{22} and M_{12} are given by

$$N_{11} = \frac{Yh}{1-\mu^2} \left[\left(\frac{1}{A_1} \frac{\partial u_1}{\partial \alpha_1} + \frac{u_2}{A_1 A_2} \frac{\partial A_1}{\partial \alpha_2} + \frac{u_3}{R_1} \right) + \mu \left(\frac{1}{A_2} \frac{\partial u_2}{\partial \alpha_2} + \frac{u_1}{A_1 A_2} \frac{\partial A_2}{\partial \alpha_1} + \frac{u_3}{R_2} \right) \right],$$
$$N_{22} = \frac{Yh}{1-\mu^2} \left[\left(\frac{1}{A_2} \frac{\partial u_2}{\partial \alpha_2} + \frac{u_1}{A_1 A_2} \frac{\partial A_2}{\partial \alpha_1} + \frac{u_3}{R_2} \right) + \mu \left(\frac{1}{A_1} \frac{\partial u_1}{\partial \alpha_1} + \frac{u_2}{A_1 A_2} \frac{\partial A_1}{\partial \alpha_2} + \frac{u_3}{R_1} \right) \right], \tag{3}$$
$$N_{12} = \frac{Yh}{2(1+\mu)} \left[\frac{A_2}{A_1} \frac{\partial}{\partial \alpha_1} \left(\frac{u_2}{A_2} \right) + \frac{A_1}{A_2} \frac{\partial}{\partial \alpha_2} \left(\frac{u_1}{A_1} \right) \right],$$

$$
\begin{aligned}
M_{11} &= D\Bigg\{\left[\frac{1}{A_1}\frac{\partial}{\partial\alpha_1}\left(\frac{u_1}{R_1}-\frac{1}{A_1}\frac{\partial u_3}{\partial\alpha_1}\right)+\frac{1}{A_1A_2}\left(\frac{u_2}{R_2}-\frac{1}{A_2}\frac{\partial u_3}{\partial\alpha_2}\right)\frac{\partial A_1}{\partial\alpha_2}\right]\\
&\quad+\mu\left[\frac{1}{A_2}\frac{\partial}{\partial\alpha_2}\left(\frac{u_2}{R_2}-\frac{1}{A_2}\frac{\partial u_3}{\partial\alpha_2}\right)+\frac{1}{A_1A_2}\left(\frac{u_1}{R_1}-\frac{1}{A_1}\frac{\partial u_3}{\partial\alpha_1}\right)\frac{\partial A_2}{\partial\alpha_1}\right]\Bigg\},\\
M_{22} &= D\Bigg\{\left[\frac{1}{A_2}\frac{\partial}{\partial\alpha_2}\left(\frac{u_2}{R_2}-\frac{1}{A_2}\frac{\partial u_3}{\partial\alpha_2}\right)+\frac{1}{A_1A_2}\left(\frac{u_1}{R_1}-\frac{1}{A_1}\frac{\partial u_3}{\partial\alpha_1}\right)\frac{\partial A_2}{\partial\alpha_1}\right]\\
&\quad+\mu\left[\frac{1}{A_1}\frac{\partial}{\partial\alpha_1}\left(\frac{u_1}{R_1}-\frac{1}{A_1}\frac{\partial u_3}{\partial\alpha_1}\right)+\frac{1}{A_1A_2}\left(\frac{u_2}{R_2}-\frac{1}{A_2}\frac{\partial u_3}{\partial\alpha_2}\right)\frac{\partial A_1}{\partial\alpha_2}\right]\Bigg\},\\
M_{12} &= \frac{D(1-\mu)}{2}\left\{\frac{A_2}{A_1}\frac{\partial}{\partial\alpha_1}\left[\frac{1}{A_2}\left(\frac{u_2}{R_2}-\frac{1}{A_2}\frac{\partial u_3}{\partial\alpha_2}\right)\right]+\frac{A_1}{A_2}\frac{\partial}{\partial\alpha_2}\left[\frac{1}{A_1}\left(\frac{u_1}{R_1}-\frac{1}{A_1}\frac{\partial u_3}{\partial\alpha_1}\right)\right]\right\},
\end{aligned}
\tag{4}
$$

where Y and μ are the Young's modulus and Poisson's ratio respectively, and $D = Yh^3/[12(1-\mu^2)]$ is the bending stiffness of the shell. In Eq. (2), F_1^{a}, F_2^{a} and F_3^{a} are the forces induced by the actuator layer which have the following form:

$$
\begin{aligned}
F_1^{\mathrm{a}} &= \frac{1}{A_1A_2}\left[-d_{31}Y_{\mathrm{p}}\frac{\partial(A_2V)}{\partial\alpha_1}+d_{32}Y_{\mathrm{p}}\frac{\partial A_2}{\partial\alpha_1}V-\frac{1}{R_1}r_1^{\mathrm{a}}d_{31}Y_{\mathrm{p}}\frac{\partial(A_2V)}{\partial\alpha_1}+\frac{1}{R_1}r_2^{\mathrm{a}}d_{32}Y_{\mathrm{p}}\frac{\partial A_2}{\partial\alpha_1}V\right],\\
F_2^{\mathrm{a}} &= \frac{1}{A_1A_2}\left[-d_{32}Y_{\mathrm{p}}\frac{\partial(A_1V)}{\partial\alpha_2}+d_{31}Y_{\mathrm{p}}\frac{\partial A_1}{\partial\alpha_2}V-\frac{1}{R_2}r_2^{\mathrm{a}}d_{32}Y_{\mathrm{p}}\frac{\partial(A_1V)}{\partial\alpha_2}+\frac{1}{R_2}r_1^{\mathrm{a}}d_{31}Y_{\mathrm{p}}\frac{\partial A_1}{\partial\alpha_2}V\right],\\
F_3^{\mathrm{a}} &= -\frac{1}{A_1A_2}\frac{\partial}{\partial\alpha_1}\left[\frac{1}{A_1}\frac{\partial}{\partial\alpha_1}(r_1^{\mathrm{a}}d_{31}Y_{\mathrm{p}}A_2V)-r_2^{\mathrm{a}}d_{32}Y_{\mathrm{p}}\frac{\partial A_2}{\partial\alpha_1}V\right]\\
&\quad-\frac{1}{A_1A_2}\frac{\partial}{\partial\alpha_2}\left[\frac{1}{A_2}\frac{\partial}{\partial\alpha_2}(r_2^{\mathrm{a}}d_{32}Y_{\mathrm{p}}A_1V)-r_1^{\mathrm{a}}d_{31}Y_{\mathrm{p}}\frac{\partial A_1}{\partial\alpha_2}V\right]+\left(\frac{d_{31}Y_{\mathrm{p}}V}{R_1}+\frac{d_{32}Y_{\mathrm{p}}V}{R_2}\right),
\end{aligned}
\tag{5}
$$

where d_{31} and d_{32} are the piezoelectric strain constants of the actuator layer, V is the voltage applied on the actuator, Y_{p} the Young's modulus of the actuator layer, r_1^{a} and r_2^{a} are the z coordinates measured from the neutral surface to the mid-surface of the actuator layer.

When N_{s} piezoelectric sensor patches are bonded on the host shell instead of the one sensor lamina, the output voltage of each patches becomes

$$
\begin{aligned}
V_i^{\mathrm{s}} &= -\frac{h_{si}}{\epsilon_{33i}S_i^{\mathrm{e}}}\int\int_{S_i^{\mathrm{e}}}\Bigg\{\left[e_{31i}\left(\frac{1}{A_1}\frac{\partial u_1}{\partial\alpha_1}+\frac{u_2}{A_1A_2}\frac{\partial A_1}{\partial\alpha_2}+\frac{u_3}{R_1}\right)+e_{32i}\left(\frac{1}{A_2}\frac{\partial u_2}{\partial\alpha_2}+\frac{u_1}{A_1A_2}\frac{\partial A_2}{\partial\alpha_1}+\frac{u_3}{R_2}\right)\right]\\
&\quad+e_{31i}r_{1i}^{\mathrm{s}}\left[\frac{1}{A_1}\frac{\partial}{\partial\alpha_1}\left(\frac{u_1}{R_1}-\frac{1}{A_1}\frac{\partial u_3}{\partial\alpha_1}\right)+\frac{1}{A_1A_2}\left(\frac{u_2}{R_2}-\frac{1}{A_2}\frac{\partial u_3}{\partial\alpha_2}\right)\frac{\partial A_1}{\alpha_2}\right]\\
&\quad+e_{32i}r_{2i}^{\mathrm{s}}\left[\frac{1}{A_2}\frac{\partial}{\partial\alpha_2}\left(\frac{u_2}{R_2}-\frac{1}{A_2}\frac{\partial u_3}{\partial\alpha_2}\right)+\frac{1}{A_1A_2}\left(\frac{u_1}{R_1}-\frac{1}{A_1}\frac{\partial u_3}{\partial\alpha_1}\right)\frac{\partial A_2}{\partial\alpha_1}\right]\Bigg\}A_1A_2\,\mathrm{d}\alpha_1\,\mathrm{d}\alpha_2\\
&\quad i=1,2,\ldots,N_{\mathrm{s}},
\end{aligned}
\tag{6}
$$

where the subscript i denotes the ith sensor wafer.

For the case that N_{a} actuator patches are bonded discretely on the host shell and an uniform voltage is applied on each patch, the voltage distribution in Eq. (5) can be expressed as

$$
V(\alpha_1,\alpha_2,t)=\sum_{j=1}^{N_{\mathrm{a}}}V_j(t)H_j,
\tag{7}
$$

where

$$
H_j=[H(\alpha_1-\alpha_{lj})-H(\alpha_1-\alpha_{rj})][H(\alpha_2-\alpha_{bj})-H(\alpha_2-\alpha_{tj})],\quad j=1,2,\ldots,N_{\mathrm{a}}
\tag{8}
$$

in which $H(\cdot)$ is the Heaviside step function, and α_{lj}, α_{rj}, α_{bj} and α_{tj} are the boundary coordinates of the jth actuator patches. Eqs. (1) and (2) are the sensor equation and the actuator equation respectively, which are the basic equations for vibration control of the smart shell.

3. Modal coordinates estimation for smart shell

To perform the modal control of the shell, the modal coordinates and velocities for the modes to be controlled should be observed. The modal coordinates will be estimated from the outputs of the sensor patches by the quasi-modal sensor, and a criterion for finding the optimal placement and sizing of the sensor patches will be given to minimize the errors of the estimation.

3.1. Quasi-modal sensor design

The displacements of the shell can be expanded as the superposition of the modes:

$$u_m(\alpha_1,\alpha_2,t)=\sum_{k=1}^{\infty}\eta_k(t)U_{mk}(\alpha_1,\alpha_2)\quad m=1,2,3, \tag{9}$$

where $\eta_k(t)$ is the kth modal coordinate of the smart shell, and $U_{mk}(\alpha_1,\alpha_2)$ is the modal shape function. Substituting Eq. (9) into Eq. (6), we have

$$V_i^{\mathrm{s}}(t)=\sum_{k=1}^{\infty}b_{ik}\eta_k(t), \tag{10}$$

where

$$\begin{aligned}b_{ik}=-\frac{h_{si}}{\epsilon_{33i}S_i^{\mathrm{e}}}\int\int_{S_i^{\mathrm{e}}}\Bigg\{&\left[e_{31i}\left(\frac{1}{A_1}\frac{\partial U_{1k}}{\partial\alpha_1}+\frac{U_{2k}}{A_1A_2}\frac{\partial A_1}{\partial\alpha_2}+\frac{U_{3k}}{R_1}\right)+e_{32i}\left(\frac{1}{A_2}\frac{\partial U_{2k}}{\partial\alpha_2}+\frac{U_{1k}}{A_1A_2}\frac{\partial A_2}{\partial\alpha_1}+\frac{U_{3k}}{R_2}\right)\right]\\&+e_{31i}r_{1i}^{\mathrm{s}}\left[\frac{1}{A_1}\frac{\partial}{\partial\alpha_1}\left(\frac{U_{1k}}{R_1}-\frac{1}{A_1}\frac{\partial U_{3k}}{\partial\alpha_1}\right)+\frac{1}{A_1A_2}\left(\frac{U_{2k}}{R_2}-\frac{1}{A_2}\frac{\partial U_{3k}}{\partial\alpha_2}\right)\frac{\partial A_1}{\partial\alpha_2}\right]\\&+e_{32i}r_{2i}^{\mathrm{s}}\left[\frac{1}{A_2}\frac{\partial}{\partial\alpha_2}\left(\frac{U_{2k}}{R_2}-\frac{1}{A_2}\frac{\partial U_{3k}}{\partial\alpha_2}\right)+\frac{1}{A_1A_2}\left(\frac{U_{1k}}{R_1}-\frac{1}{A_1}\frac{\partial U_{3k}}{\partial\alpha_1}\right)\frac{\partial A_2}{\partial\alpha_1}\right]\Bigg\}A_1A_2\,\mathrm{d}\alpha_1\,\mathrm{d}\alpha_2\end{aligned} \tag{11}$$

are the coefficients related to the locations and sizes of the sensor elements and the modal functions of the shell.

Making truncation, and only the first M ($M>\max(N_{\mathrm{a}},N_{\mathrm{s}})$ is a large integer) modes of the shell being considered, Eq. (10) becomes

$$\{V^{\mathrm{s}}(t)\}=[B]\{\eta(t)\}, \tag{12}$$

where $\{V^{\mathrm{s}}(t)\}\in R^{N_{\mathrm{s}}}$ is a vector of output voltages generated by the sensor elements, $\{\eta(t)\}\in R^{M}$ a vector containing the first M modal coordinates of the shell, and $[B]\in R^{N_{\mathrm{s}}M}$ a matrix related to the output charges of the sensor elements and the modal coordinates.

Eq. (12) establishes the relation between the sensor outputs and the modal coordinates which can be used to estimate the lower N_{s} modal coordinates approximately. To this end, rewrite Eq. (12) as

$$\{V^{\mathrm{s}}(t)\}=[B_1]\{\eta_1(t)\}+[\mathrm{B}_2]\{\eta_2(t)\}, \tag{13}$$

where $[B_1]\in R^{N_{\mathrm{s}}N_{\mathrm{s}}}$ and $[B_2]\in R^{N_{\mathrm{s}}(M-N_{\mathrm{s}})}$ are the matrices composed of the first N_{s} columns and the residual entries of $[B]$, respectively, and $\{\eta_1(t)\}\in R^{N_{\mathrm{s}}}$ and $\{\eta_2(t)\}\in R^{M-N_{\mathrm{s}}}$, the vectors composed of the first N_{s} modal coordinates and the remaining $M-N_{\mathrm{s}}$ modal coordinates, respectively.

Matrix $[B_1]$ can be made nonsingular by properly placing the piezoelectric sensor patches, and therefore, we have

$$\{\eta_1(t)\} = [B_1]^{-1}\{V^s(t)\} - [B_1]^{-1}[B_2]\{\eta_2(t)\}. \tag{14}$$

In general, the magnitudes of the modal coordinates with high order are much smaller than those of the low modal coordinates. For this reason, neglecting the second term on the right-hand side of Eq. (14) leads to the following approximate equation:

$$\{\eta_1^*(t)\} = [B_1]^{-1}\{V^s(t)\}, \tag{15}$$

where $\{\eta_1^*(t)\}$ is the vector containing the N_s observed modal coordinates which is different slightly from $\{\eta_1(t)\}$. The relation between the observed and the real modal coordinates can be expressed as

$$\{\eta_1^*(t)\} = \{\eta_1(t)\} + [B_1]^{-1}[B_2]\{\eta_2(t)\}. \tag{16}$$

Eq. (16) indicates that the estimated modal coordinates obtained from Eq. (15) are equal to the real ones mixed with the residual modal coordinates with higher frequencies. The observed modal coordinates from Eq. (15) contain the remaining modal coordinates, which is referred to as observation spillover. Therefore, the above process to estimate modal coordinates is called quasi-modal sensors.

Although the quasi-modal sensor cannot give the exact modal coordinates, it separates the lowest N_s modal coordinates from each other so that the residual modal components can be easily removed by low pass filters.

3.2. Optimal placement and sizing of the sensor patches

The error vector of the estimated modal coordinates is given by

$$\{\Delta(t)\} = [B_1]^{-1}[B_2]\{\eta_2(t)\}, \tag{17}$$

and its norm can be expressed as

$$\|\Delta(t)\|^2 = \{\Delta(t)\}^T\{\Delta(t)\} = \{\eta_2(t)\}^T[B_e]\{\eta_2(t)\}, \tag{18}$$

where

$$[B_e] = [B_2]^T([B_1]^{-1})^T[B_1]^{-1}[B_2] \tag{19}$$

is a $(M - N_s)(M - N_s)$ symmetric positive definite matrix.

It can be proved that the following inequality holds:

$$\|\Delta(t)\|^2 \leqslant \lambda_{\max}([B_e])\{\eta_2(t)\}^T\{\eta_2(t)\}, \tag{20}$$

where $\lambda_{\max}([B_e])$ is the maximum eigenvalue of $[B_e]$.

To minimize the observation spillover for any $\{\eta_2(t)\}$ in Eq. (20), the maximum eigenvalue of $[B_e]$ should be minimized, i.e.

$$J_s = \min_{S_i^e (i=1,2,\ldots,N_s)} \lambda_{\max}\{[B_e]\}. \tag{21}$$

Eq. (21) is the criterion using which the optimal locations and sizes of the sensor elements can be obtained. The observation spillover can be greatly decreased by optimal placement of the piezoelectric sensor patches.

4. Quasi-modal actuator design for smart shells

4.1. Quasi-modal actuator design

Substituting Eqs. (3), (4) and (9) into Eq. (2), and employing the mode orthogonality, the modal equations of motion for a smart shell can be obtained

$$\ddot{\eta}_k(t) + \omega_k^2 \eta_k(t) = \sum_{j=1}^{N_a} c_{kj} V_j(t), \quad k = 1, 2, \ldots, \tag{22}$$

where ω_k is the kth natural frequency of the shell, and

$$c_{kj} = \frac{1}{\rho h N_k} \int_{\alpha_1} \int_{\alpha_2} \left(\sum_{m=1}^{3} F_m^e(H_j) U_{mk}(\alpha_1, \alpha_2) \right) A_1 A_2 \, d\alpha_1 \, d\alpha_2, \tag{23}$$

where $F_m^e(H_j)$ can be obtained by replacing V with H_j in Eq. (5), and N_k is given by

$$N_k = \int_{\alpha_1} \int_{\alpha_2} \left(\sum_{m=1}^{3} U_{mk}^2(\alpha_1, \alpha_2) \right) A_1 A_2 \, d\alpha_1 \, d\alpha_2. \tag{24}$$

The constants c_{kj} in Eq. (23) are referred to as the modal influence coefficients, which depend on both the modal shape functions and the locations and sizes of the actuator elements.

When only the first M modes are considered, Eq. (22) can be written in the following matrix form:

$$\begin{aligned} \{\ddot{\eta}_c(t)\} + [\Omega_c^2]\{\eta_c(t)\} &= [C_c]\{V(t)\}, \\ \{\ddot{\eta}_r(t)\} + [\Omega_r^2]\{\eta_r(t)\} &= [C_r]\{V(t)\}, \end{aligned} \tag{25}$$

where $\{\eta_c(t)\} \in R^{N_a}$ and $\{\eta_r(t)\} \in R^{M-N_a}$ are the vectors of the N_a controlled modes and the $M - N_a$ uncontrolled (residual) modes respectively, $\{V(t)\} \in R^{N_a}$ is a vector composed of the voltages applied on the piezoelectric actuator elements, $[\Omega_c^2] = \mathrm{diag}(\omega_1^2, \omega_2^2, \ldots, \omega_{N_a}^2)$, $[\Omega_r^2] = \mathrm{diag}(\omega_{N_a+1}^2, \omega_{N_a+2}^2, \ldots, \omega_M^2)$, and $[C_c] \in R^{N_a N_a}$ and $[C_r] \in R^{(M-N_a)N_a}$ are the modal influence matrices composed of the entries related to the controlled and residual modes respectively.

For the modes to be controlled, by applying adequate control voltages, the piezoelectric actuator patches should be capable of producing the expected modal control forces. If the modal forces for the N_a controlled modes are designated to be $\{f_c(t)\} = [f_1(t), f_2(t), \ldots, f_{N_a}(t)]^T$, then the voltages that can generate such N_a modal forces satisfy the following equations:

$$[C_c]\{V(t)\} = \{f_c(t)\}. \tag{26}$$

The matrix $[C_c]$ can be made nonsingular by properly configuring the actuators, and therefore the voltages applied on the actuators can be obtained as

$$\{V(t)\} = [C_c]^{-1}\{f_c(t)\}, \tag{27}$$

which gives the voltage distribution to generate the designated modal forces.

It should be pointed out that the voltage designated for the controlled modes will excite the residual modes, i.e. the control spillover will occur. Therefore, the process given above to generate the designated modal forces by modulating the voltage distribution is called quasi-modal actuator.

4.2. Control spillover estimate and optimal placement of the actuator patches

To estimate the degree of the control spillover, substituting Eq. (27) into the second equation of Eq. (25), the spillover modal forces $\{f_r(t)\}$ for the $M - N_a$ residual modes can be given as

$$\{f_r(t)\} = [C_r][C_c]^{-1}\{f_c(t)\}. \tag{28}$$

The norm of the spillover modal forces can be obtained as

$$\|f_r(t)\|^2 = \{f_r(t)\}^T\{f_r(t)\} = \{f_c(t)\}^T[C_s]\{f_c(t)\}, \tag{29}$$

where

$$[C_s] = \left([C_c]^{-1}\right)^T[C_r]^T[C_r][C_c]^{-1} \tag{30}$$

is a $N_a \times N_a$ real symmetric square matrix related to the control spillover. It can be proved that

$$\|f_r(t)\|^2 \leqslant \lambda_{max}([C_s])\{f_c(t)\}^T\{f_c(t)\}, \tag{31}$$

where $\lambda_{max}([C_s])$ is the maximum eigenvalue of $[C_s]$. Eq. (31) indicates that a smaller maximum eigenvalue of $[C_s]$ will decrease the control spillover, which will be used as a controlling factor to obtain the optimal placement of the actuator patches.

For the actuator patches, in addition to the control spillover problem, the most important factor for the optimal placement of actuators is how to use less control energy to produce the designated modal forces. To this end, consider the relation between the modal control forces and the control voltages, which can be obtained as follows from Eq. (26):

$$\{f_c(t)\}^T\{f_c(t)\} = \{V(t)\}^T[C_c]^T[C_c]\{V(t)\}, \tag{32}$$

where $[C_c]^T[C_c]$ is a symmetric square positive definite matrix. Once again, it can be proved that

$$\|V(t)\|^2 = \{V(t)\}^T\{V(t)\} \leqslant \{f_c(t)\}^T\{f_c(t)\}/\lambda_{min}([C_c]^T[C_c]), \tag{33}$$

where $\lambda_{min}([C_c]^T[C_c])$ is the minimum eigenvalue of the matrix $[C_c]^T[C_c]$. It can be seen from inequality (33) that for any given modal control forces $\{f_c(t)\}$, a larger minimum eigenvalue of $[C_c]^T[C_c]$ will result in smaller control voltages. Combining inequalities (31) and (33), the following criterion can be given

$$J_a = \min_{S_{aj}(j=1,2,\ldots,N_a)} Q_1\lambda_{max}([C_s]) - Q_2\lambda_{min}([C_c]^T[C_c]), \tag{34}$$

where Q_1 and Q_2 are weighting coefficients. In general, $\lambda_{min}([C_c]^T[C_c])$ is much smaller than $\lambda_{max}([C_s])$, therefore, Q_2 should be selected much larger than Q_1 so that both control efficiency and control spillover are well balanced during optimization. The optimal locations and sizes of the N_a piezoelectric actuator elements can be obtained using criterion (34).

5. Modal control of smart shell

Based on the quasi-modal sensor and quasi-modal actuator, the modal control of the smart shell can be performed. However, the modal coordinates observed by the quasi-modal sensor cannot be used directly because the observation spillover may destabilize the closed-loop system. To solve this problem, the first step is to optimally placing the sensor elements to decrease the observation spillover, and the second step is to filter the residual components during the control process. In this section, the independent positive po-

sition feedback control method is used to control the first N_a modes of the smart shell independently. For each mode to be controlled, a compensator is designed as follows (Fanson and Caughey, 1990):

$$\ddot{\xi}_i(t) + 2\zeta_{ci}\omega_i\dot{\xi}_i(t) + \omega_i^2\xi_i(t) = \omega_i^2\eta_i^*(t), \quad i = 1, 2, \ldots, N_a, \tag{35}$$

where $\xi_i(t)$ is the response of the ith compensator to the estimated modal coordinate $\eta_i^*(t)$, ζ_{ci} the damping ratio of the compensator. The control forces for the first N_a modes are designed according to the following control law:

$$f_i(t) = g_i\xi_i(t), \tag{36}$$

where $g_i \geqslant 0$ is the control gain. In this case, the control gains can be easily selected because the active damping ratio of each controlled mode is approximately proportional to the corresponding control gain. However, the control gains should be carefully selected so that the control voltage on each actuator element is limited in an appropriate range.

The compensator in Eq. (35) has two functions, one is that it can remove the components with frequencies higher than ω_i from the estimated modal coordinate η_i^* and only the signal with frequency ω_i can pass through. In other words, the compensator acts as a low pass filter through which the observation spillover can be suppressed.

Another function of the compensator is to change the phase of the modal coordinate. The response $\xi_i(t)$ of the compensator is 180° out of the ith modal velocity $\dot{\eta}_i(t)$ because of the resonance. The phase shift function of the compensator makes the control easier because it is unnecessary to observe the modal velocities. Therefore, the control law in Eq. (36) can provide the active damping to the controlled modes, although the modal velocities are not observed directly.

6. Case study: cylindrical shell

Consider a smart cylindrical shell with radius R and thickness h. Assume that $d_{32} = d_{31}$. In this case, α_1 and α_2 are replaced by the width direction coordinate x and the circumferential direction coordinate φ. The Lame parameters are $A_1 = 1$ and $A_2 = R$, and the radii are $R_1 = \infty$, and $R_2 = R$.

The sensor equation of the cylindrical shell can be simplified from Eq. (1) as follows:

$$V^s = -\frac{h_s}{\epsilon_{33}S^e}\int\int_{S^e}\left[e_{31}\frac{\partial u_1}{\partial x} + \frac{e_{32}}{R}\left(\frac{\partial u_2}{\partial\varphi} + u_3\right) - e_{31}r_s\frac{\partial^2 u_3}{\partial x^2} + \frac{e_{32}r_s}{R^2}\left(\frac{\partial u_2}{\partial\varphi} - \frac{\partial^2 u_3}{\partial\varphi^2}\right)\right]A_1A_2\,\mathrm{d}\alpha_1\,\mathrm{d}\alpha_2. \tag{37}$$

Substituting the above parameters into Eqs. (2)–(4), and making some simplification, the differential equations of motion for the cylindrical shell can be expressed as

$$\begin{aligned}
&\frac{\partial^2 u_1}{\partial x^2} + \frac{1-\mu}{2R^2}\frac{\partial^2 u_1}{\partial\varphi^2} + \frac{1+\mu}{2R}\frac{\partial^2 u_2}{\partial x\,\partial\varphi} + \frac{\mu}{R}\frac{\partial u_3}{\partial x} + \frac{(1-\mu^2)}{Yh}F_1^a = \frac{(1-\mu^2)}{Y}\rho\ddot{u}_1,\\
&\frac{1+\mu}{2}\frac{\partial^2 u_1}{\partial x\,\partial\varphi} + R\frac{1-\mu}{2}\frac{\partial^2 u_2}{\partial x^2} + \frac{1}{R}\frac{\partial^2 u_2}{\partial\varphi^2} + \frac{1}{R}\frac{\partial u_3}{\partial\varphi} + \frac{(1-\mu^2)R}{Yh}F_2^a = \frac{(1-\mu^2)R}{Y}\rho\ddot{u}_2,\\
&\mu\frac{\partial u_1}{\partial x} + \frac{1}{R}\frac{\partial u_2}{\partial\varphi} + \frac{u_3}{R} + \frac{h^2R}{12}\left(\frac{\partial^4 u_3}{\partial x^4} + \frac{2}{R^2}\frac{\partial^4 u_3}{\partial x^2\,\partial\varphi^2} + \frac{1}{R^4}\frac{\partial^4 u_3}{\partial\varphi^4}\right) - \frac{(1-\mu^2)R}{Yh}F_3^a = -\frac{(1-\mu^2)R}{Y}\rho\ddot{u}_3,
\end{aligned} \tag{38}$$

where the actuating forces F_1^a, F_2^a and F_3^a are given by

$$F_1^a = -d_{31} Y_p \frac{\partial V}{\partial x},$$
$$F_2^a = -\left(1 + \frac{r_a}{R}\right) \frac{d_{31} Y_p}{R} \frac{\partial V}{\partial \varphi}, \tag{39}$$
$$F_3^a = -r_a d_{31} Y_p \frac{\partial^2 V}{\partial x^2} - \frac{r_a}{R^2} d_{31} Y_p \frac{\partial^2 V}{\partial \varphi^2} + \frac{d_{31} Y_p V}{R}.$$

Eq. (39) gives the relationship between the actuating forces and the applied voltage on the piezoelectric actuator layer for the cylindrical shell.

6.1. Case 1: a closed-form cylindrical shell

For a closed-form cylindrical shell simply supported at both ends, the displacements can be expressed as

$$u_1(x, \varphi, t) = \sum_{m=1}^{\infty} \sum_{n=1}^{\infty} \eta_{mn}(t) U_{mn} \cos \frac{m\pi x}{l} \cos n\varphi,$$
$$u_2(x, \varphi, t) = \sum_{m=1}^{\infty} \sum_{n=1}^{\infty} \eta_{mn}(t) V_{mn} \sin \frac{m\pi x}{l} \sin n\varphi, \tag{40}$$
$$u_3(x, \varphi, t) = \sum_{m=1}^{\infty} \sum_{n=1}^{\infty} \eta_{mn}(t) W_{mn} \sin \frac{m\pi x}{l} \cos n\varphi,$$

where U_{mn}, V_{mn} and W_{mn} are constants. The frequency equation can be derived as

$$\begin{vmatrix} \beta_{11} - \lambda^2 & \beta_{12} & \beta_{13} \\ \beta_{12} & \beta_{22} - \lambda^2 & \beta_{23} \\ \beta_{13} & \beta_{23} & \beta_{33} - \lambda^2 \end{vmatrix} = 0, \tag{41}$$

where $\lambda^2 = (1 - \mu^2)\rho\omega^2 / Y$, and the entries are given by

$$\beta_{11} = \left(\frac{m\pi}{l}\right)^2 + \frac{(1-\mu^2)n^2}{2R^2}, \qquad \beta_{12} = -\frac{1+\mu}{2R} \frac{m\pi n}{l}, \qquad \beta_{13} = -\frac{\mu m\pi}{Rl},$$
$$\beta_{22} = \frac{1-\mu}{2}\left(\frac{m\pi}{l}\right)^2 + \frac{n^2}{R^2}, \qquad \beta_{23} = \frac{n}{R^2}, \qquad \beta_{33} = \frac{1}{R^2} + \frac{h^2}{12}\left[\left(\frac{m\pi}{l}\right)^2 + \frac{n^2}{R^2}\right]^2. \tag{42}$$

6.2. Case 2: an open-form cylindrical shell

For an open-form cylindrical shell with all four edges simply supported, its displacements can expanded as the following form:

$$u_1(x, \varphi, t) = \sum_{m=1}^{\infty} \sum_{n=1}^{\infty} \eta_{mn}(t) U_{mn} \cos \frac{m\pi x}{l} \sin \frac{n\pi\varphi}{\Phi},$$
$$u_2(x, \varphi, t) = \sum_{m=1}^{\infty} \sum_{n=1}^{\infty} \eta_{mn}(t) V_{mn} \sin \frac{m\pi x}{l} \cos \frac{n\pi\varphi}{\Phi}, \tag{43}$$
$$u_3(x, \varphi, t) = \sum_{m=1}^{\infty} \sum_{n=1}^{\infty} \eta_{mn}(t) W_{mn} \sin \frac{m\pi x}{l} \sin \frac{n\pi\varphi}{\Phi},$$

where Φ is the central angle subtended by the shell. In this case, the entries in frequency equation (41) are replaced by

$$\beta_{11} = \left(\frac{m\pi}{l}\right)^2 + \frac{1-\mu^2}{2R^2}\left(\frac{n\pi}{\Phi}\right)^2, \qquad \beta_{12} = \frac{1+\mu}{2R}\frac{mn\pi^2}{l\Phi}, \qquad \beta_{13} = -\frac{\mu m\pi}{Rl},$$
$$\beta_{22} = \frac{1-\mu}{2}\left(\frac{m\pi}{l}\right)^2 + \frac{n^2\pi^2}{R^2\Phi^2}, \qquad \beta_{23} = -\frac{n\pi}{R^2\Phi}, \qquad \beta_{33} = \frac{1}{R^2} + \frac{h^2}{12}\left[\left(\frac{m\pi}{l}\right)^2 + \frac{n^2\pi^2}{R^2\Phi^2}\right]^2. \tag{44}$$

7. Numerical examples

7.1. Case 1: simply supported closed-form cylindrical shell

As an illustrative example, consider a simply supported closed cylindrical shell onto which five lead zirconate titanate (PZT) actuator elements and six polyvinylidene fluoride (PVDF) sensor elements are bonded. The material properties and dimensions of the system are shown in Table 1.

The first (lowest) 10 frequencies of the cylindrical shell are 1057.1, 1113.7, 1132.6, 1271.8, 1381.9, 1505.7, 1797.8, 1802.9, 1863.2 and 1880.9 rad/s, respectively.

In order to suppress the observation spillover of the quasi-modal sensor, the locations and sizes of the six sensor elements are optimized using criterion (21). When taking $M = 10$ and assuming that each sensor elements is not larger than 6×6 cm^2 and not less than 3×3 cm^2, the optimal locations and sizes of the six sensor elements can be obtained as listed in Table 2. When the weighting coefficients are chosen as $Q_1 = 0.1$, $Q_2 = 10^5$ in criterion (34), and the same constraints are considered as the sensor optimization, the obtained optimal locations and sizes of the five actuators are also tabulated in Table 2.

With the optimum placement and sizes of the sensor and actuator elements, the modal control of the smart shell can be performed. The initial vibration of the shell is caused by the sudden removal of a force of 300 N acted at the point (0.4 m, $\pi/18$). The vibration of the shell will not decay if without control since no damping is considered. To control the first five modes, the control gains are chosen as $g_1 = 10000$, $g_2 = 8000$, $g_3 = 12000$, $g_4 = 9000$, and $g_5 = 14000$. The damping ratios of the five compensators are all taken to be 0.2. The first six estimated modal coordinates are obtained from the six outputs of the sensor patches by using the quasi-modal sensor, as shown in Fig. 2. The estimated modal coordinates, after filtering and phase shifting by the compensators (Fig. 3), are fed back to generate the control voltage for each actuator patches, and hence, the closed-loop control system is established. The first five controlled modes are shown in Fig. 4 together with the five residual.

Table 1
Material and dimensional parameters

Item	Shell	Actuators	Sensors
Mass density (kg/m^3)	8000	7600	1780
Young's modulus (GPa)	210	63	2
Poisson's ratio	0.3	0.3	0.3
Piezo-constant d_{31} (m/V)	–	370×10^{-12}	30×10^{-12}
Thickness (m)	0.001	0.0004	0.0001
Length (m)	1.0		
Radius (m)	0.3		

Table 2
The optimum locations and sizes of the actuator and sensor elements for the closed-form cylindrical shell

Piezoelectric element number	Central coordinate (m, rad)	Length (cm)	Central angle subtended by the element (rad)
Sensor 1	(0.4279, 1.1235)	3.0695	0.1292
Sensor 2	(0.3951, 4.4922)	4.5193	0.1265
Sensor 3	(0.5190, 2.4600)	5.1552	0.1842
Sensor 4	(0.4199, 4.1451)	4.8780	0.1022
Sensor 5	(0.4324, 2.9533)	4.7208	0.1936
Sensor 6	(0.4365, 6.1231)	3.6162	0.1079
Actuator 1	(0.4400, 2.6219)	5.2438	0.1412
Actuator 2	(0.5015, 0.8360)	5.0335	0.1611
Actuator 3	(0.5042, 1.1376)	4.9011	0.2000
Actuator 4	(0.4864, 0.5045)	3.7662	0.1982
Actuator 5	(0.4446, 3.9917)	3.0007	0.1879

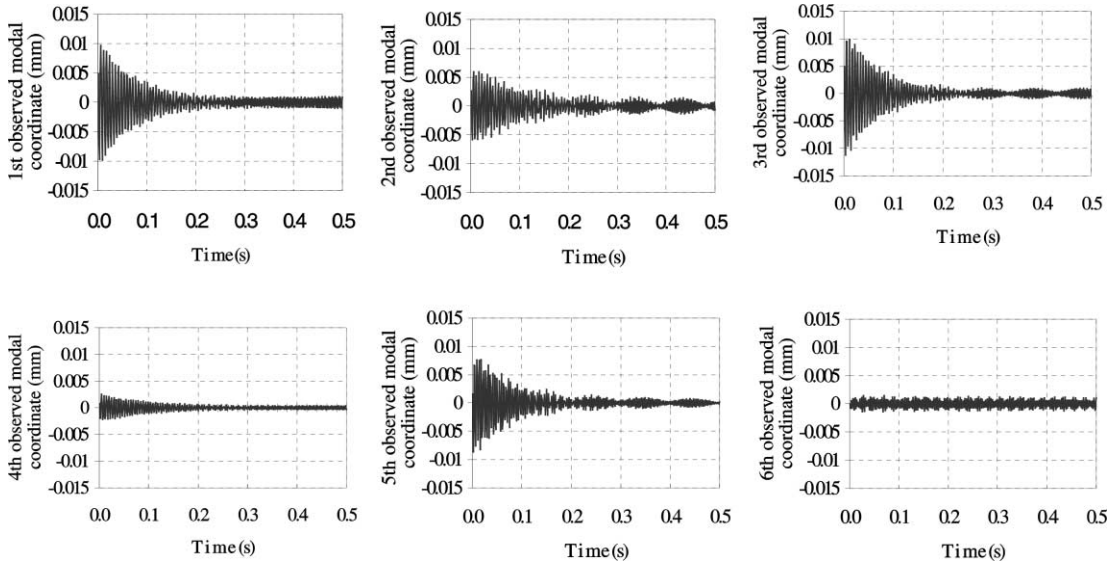

Fig. 2. The six observed modal coordinates by the quasi-modal sensor.

It can be seen from Fig. 2 that the estimated modal coordinates can be made very close the exact ones shown in Fig. 4 by using the optimal locations and sizes of the sensor elements. The remaining high frequency components in the estimated modal coordinates have been further removed by the compensators, as shown Fig. 3.

Fig. 5 gives the time history of the displacement in width direction on point (0.01 m, $\pi/3$), circumferential displacement on (0.5 m, $\pi/4$) and the transverse displacement on (0.5 m, $\pi/8$). The control voltage distribution of the optimally placed actuator elements is shown in Fig. 6. Fig. 5 shows that all the displacements of the shell in three directions are suppressed effectively in 0.5 s. Since the remaining modes are with higher frequencies than the controlled ones, they can be easily dissipated even by a light damping of the structure in practice. The control voltages in the five actuator elements are well balanced and their peak values are less than 220 V because of the optimal placement of the actuator elements.

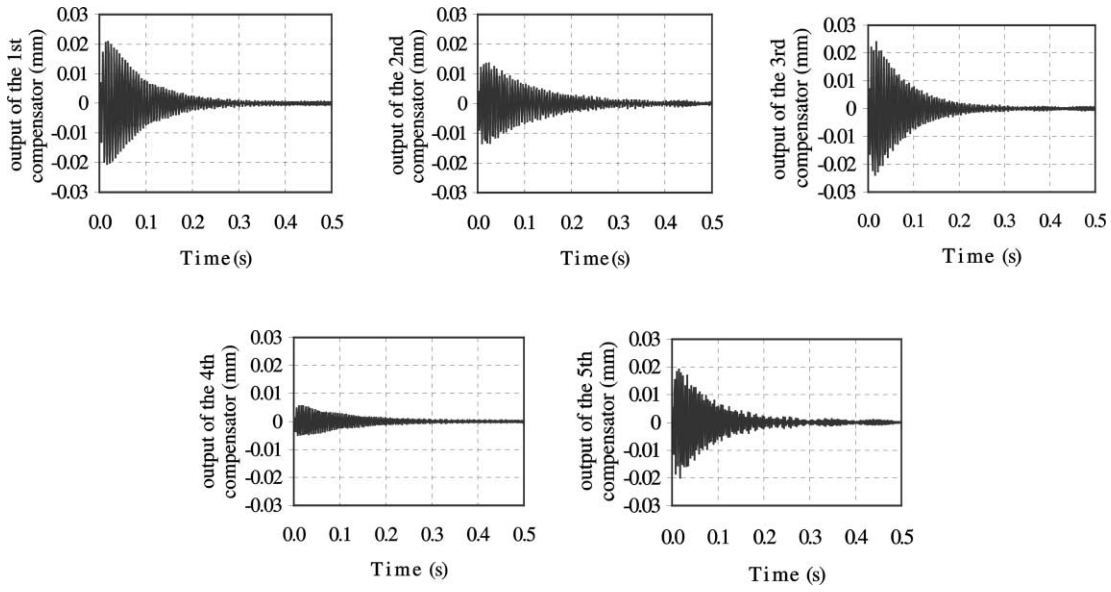

Fig. 3. The outputs of the five compensators.

7.2. Case 2: simply supported open-form cylindrical shell

As a second simulation example, consider an open portion of a cylindrical shell with four edges being simply supported. On both surfaces of the open shell six PVDF sensor elements and five PZT actuator elements are bonded respectively. The dimensions and properties are the same as the first example except that $R = 1.2$ m and $\Phi = \pi/2$.

Using Eqs. (41) and (43), the obtained lowest 10 frequencies of the curved panel are 453.45, 469.48, 472.47, 518.88, 529.89, 586.41, 650.09, 670.53, 768.28 and 807.59 rad/s, respectively. In this case, the optimization of the locations and sizes of the sensor and actuator elements are highly needed because of the close spaced modes of the open shell. The optimized locations and sizes of the sensor and elements under the constraints same as the first example are listed in Table 3.

Sudden removal of a force of 20 N acted at point (0.4 m, 0.28 rad) from the shell causes vibration of the shell, the first five modes of which will be controlled using the present method. In this example, the damping ratios of the five compensators are taken as 0.2, 0.2, 0.2, 0.1 and 0.1, and the control gains are chosen as 1500, 1200, 1200, 1000 and 1000. The first six estimated modal coordinates the outputs after filtered by the compensators, and the first ten modal coordinates are shown in Figs. 7–9. The histories of three displacements at the selected points are plotted in Fig. 10, and the control voltages applied on the actuator elements are depicted in Fig. 11.

Compared with the modal coordinates in Fig. 9, the observation spillover of the estimated modal coordinates still exists although the sensor elements have been optimally configured. After being filtered by the compensators with small damping ratios, the residual components in their outputs are decreased remarkably. Consequently, the closed-loop system is stable, as demonstrated in Figs. 9 and 10.

It should be pointed that the modal control is not as effect as the plate case (Sun et al., 1999a,b) because the slight observation spillover still exists in the outputs of the compensators due to the fact that the frequencies are closely located. Therefore, the amount of the sensor elements should be increased and much larger than that of the controlled modes for the shells with close spaced frequencies.

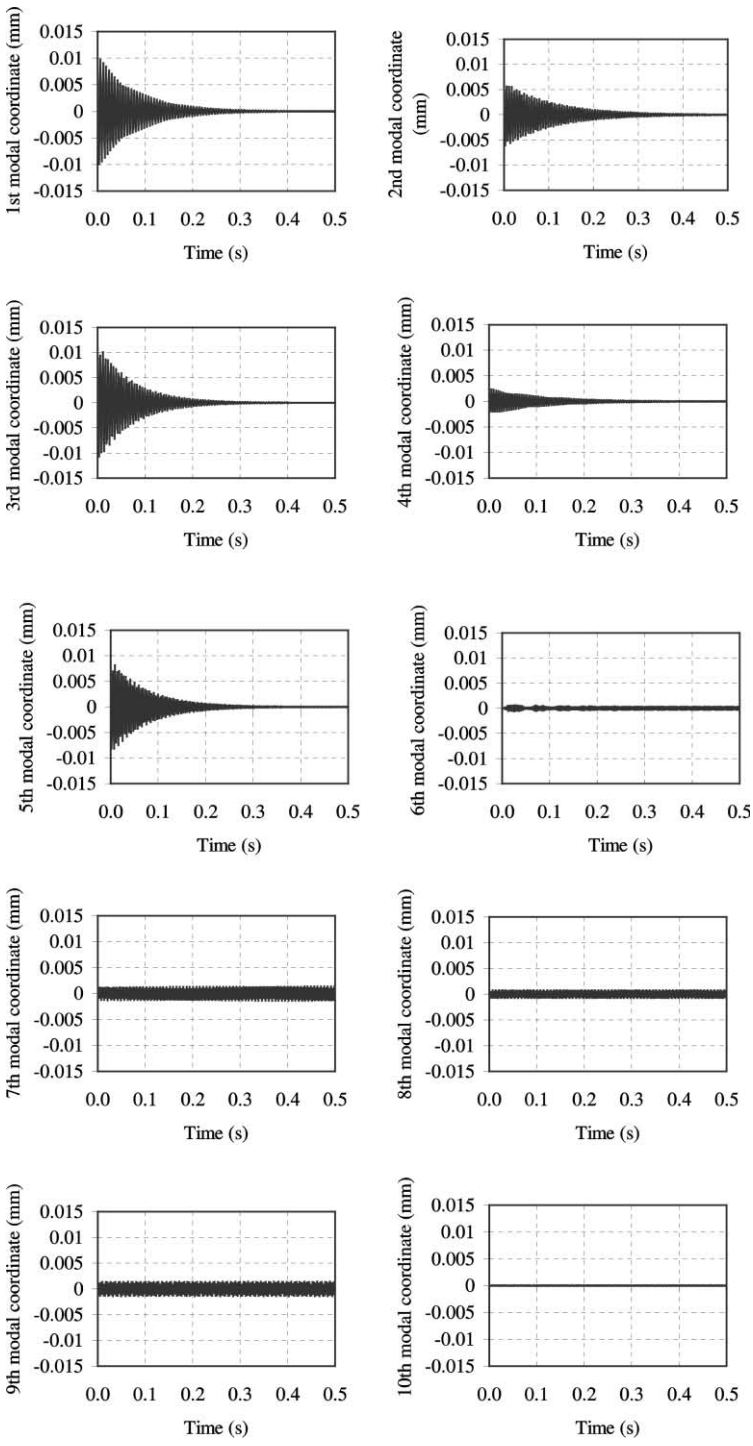

Fig. 4. The first 10 modal coordinates of the smart shell with five controlled modes.

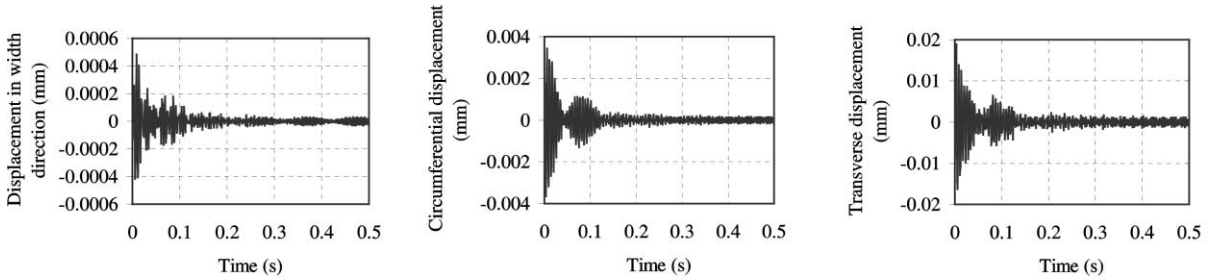

a) Displacement at point (0.01m, π/3) b) Circumferential displacement at point (0.5m, π/4) c) Transverse displacement at point (0.5m, π/8)

Fig. 5. The time history of the displacements of the shell.

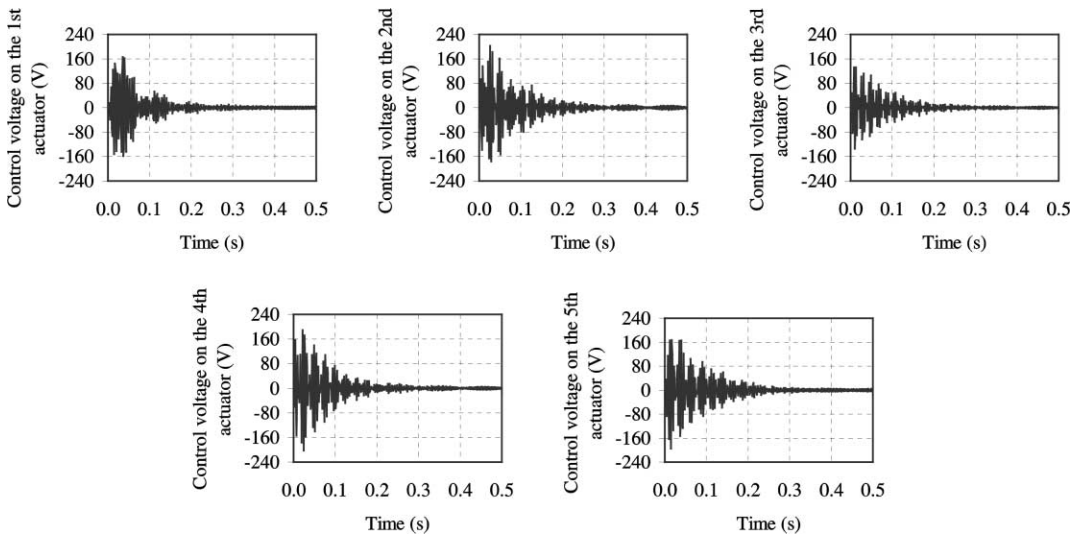

Fig. 6. The control voltage distribution on the actuator elements.

Table 3
The optimum locations and sizes of the actuator and sensor elements for the open-form cylindrical shell

Piezoelectric element number	Central coordinate (m, rad)	Length (cm)	Central angle subtended by the element (rad)
Sensor 1	(0.3346, 0.3696)	3.6944	0.0273
Sensor 2	(0.8216, 0.6307)	5.9613	0.0454
Sensor 3	(0.5702, 0.9214)	5.8494	0.0500
Sensor 4	(0.4418, 0.1239)	3.0001	0.0280
Sensor 5	(0.7452, 1.4470)	5.7224	0.0254
Sensor 6	(0.5739, 1.1937)	5.9996	0.0319
Actuator 1	(0.5224, 0.9753)	5.4475	0.0417
Actuator 2	(0.3995, 0.0834)	3.9700	0.0500
Actuator 3	(0.3167, 0.6733)	6.0000	0.0500
Actuator 4	(0.3811, 1.4677)	5.2187	0.0413
Actuator 5	(0.5605, 0.3704)	5.9992	0.0405

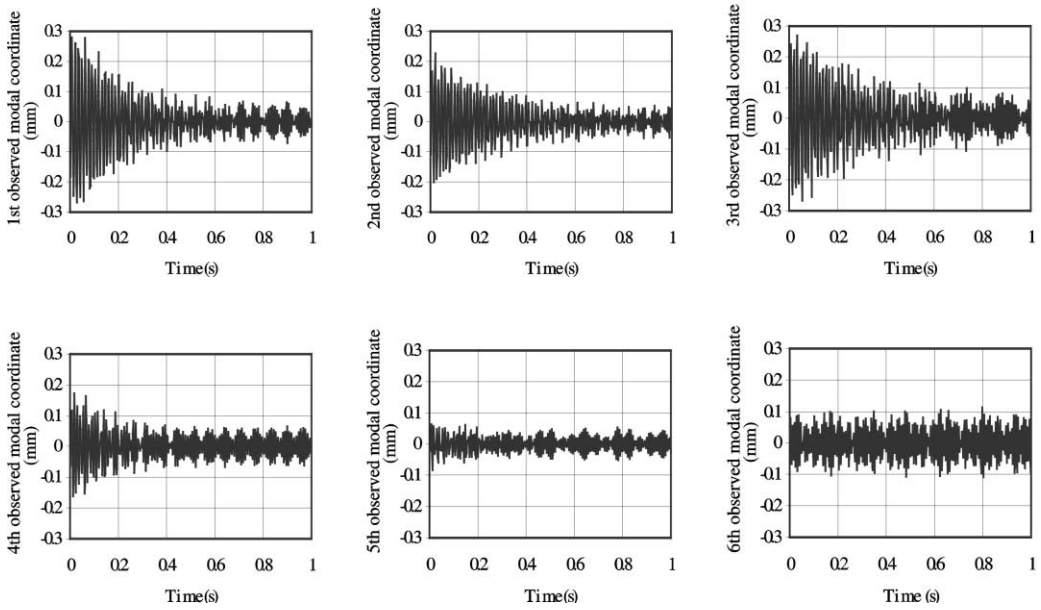

Fig. 7. The estimated modal coordinates obtained by the quasi-modal sensor.

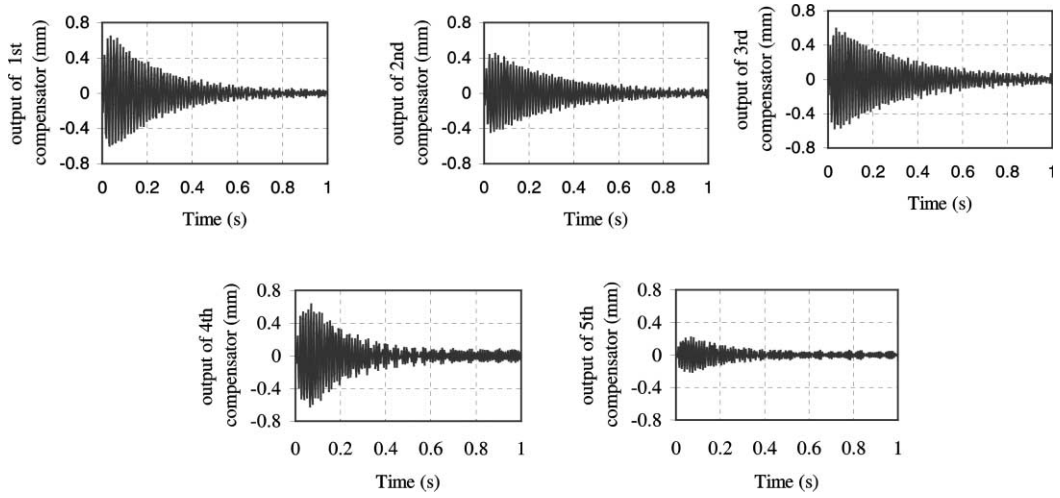

Fig. 8. The outputs of the five compensators.

The control results show that the first five modes are controlled successfully within 1 s and the peak values of the control voltages are less than 200 V. However, the entire vibration of the shell is not controlled effectively because the natural frequencies of the modes are very close and the contributions to the shell's vibration of the residual modes are important. In order to achieve satisfactory results, more modes should be controlled for the shell structures.

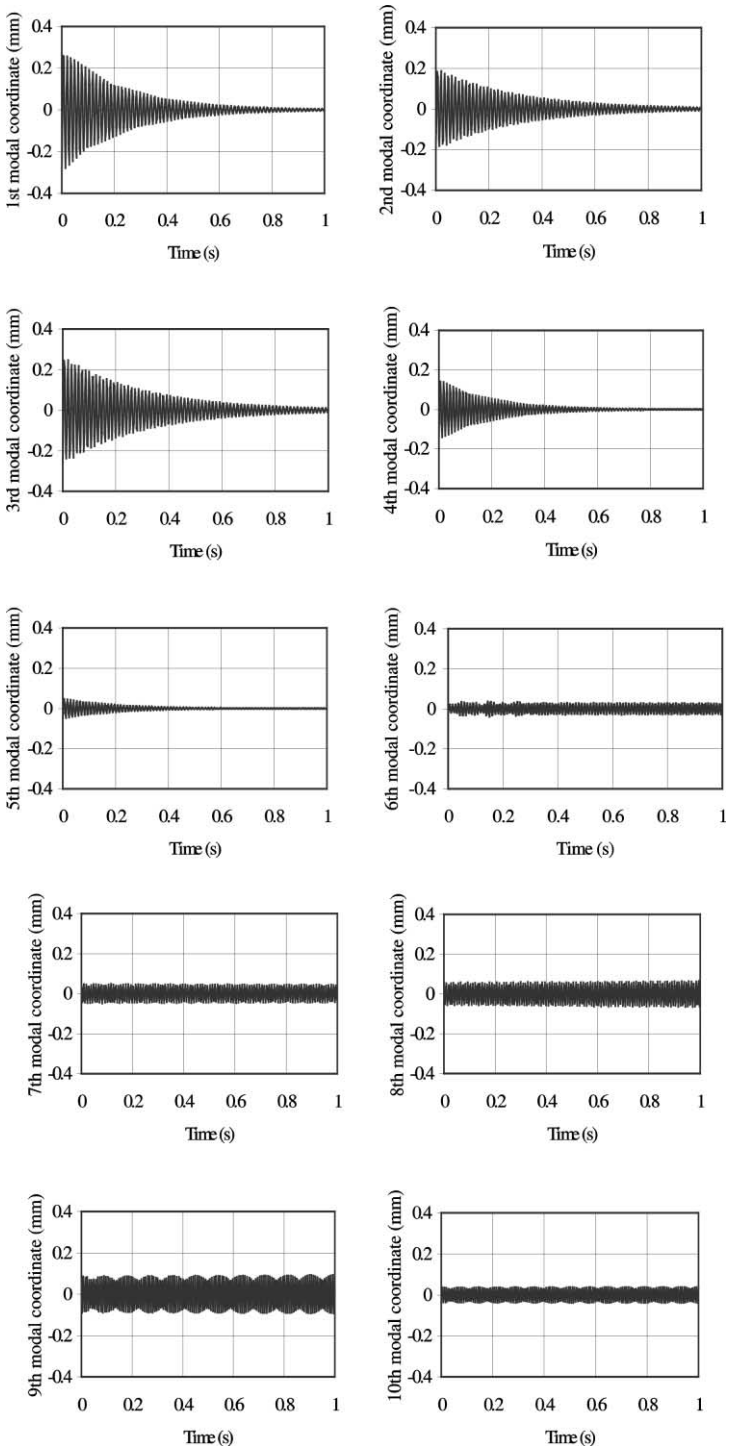

Fig. 9. The lowest 10 modal coordinates with the first five controlled modes.

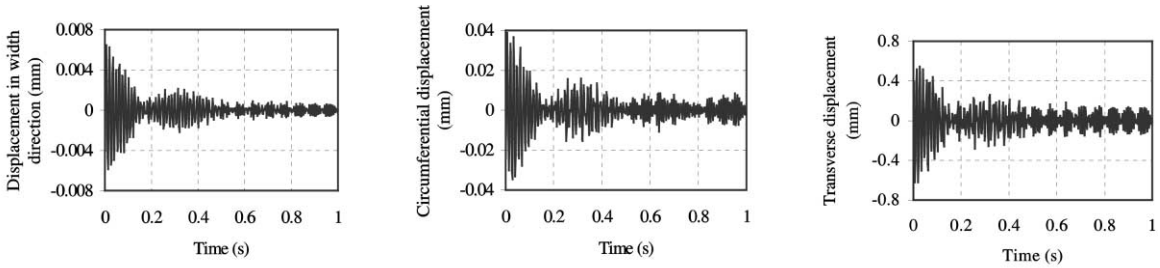

a) Displacement in width direction at point (0.01,π/10) b) Circumferential displacement at point (0.5, π/8) c) Transverse displacement at point (0.5, π/10)

Fig. 10. Time history of the displacements in three directions.

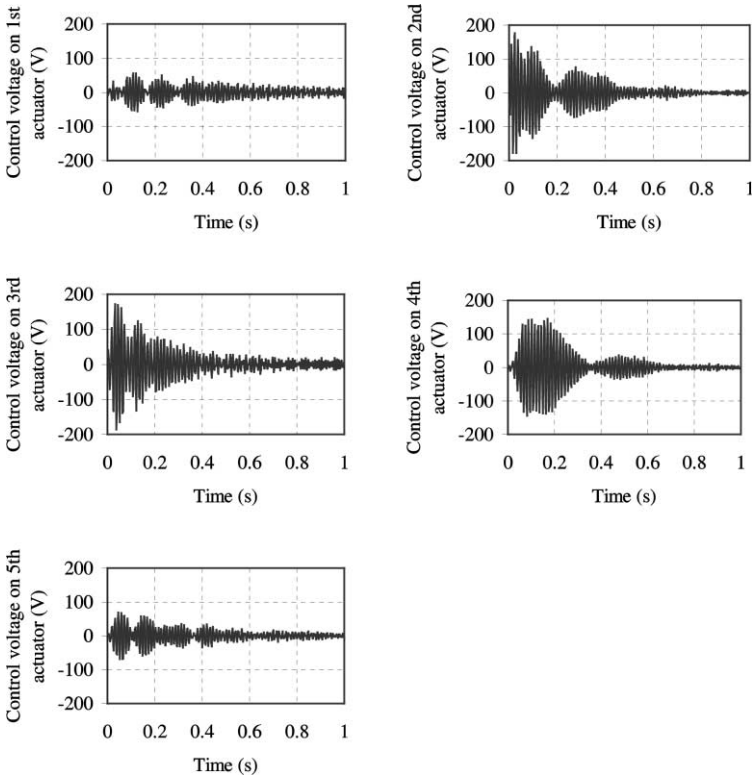

Fig. 11. The control voltage distribution on the actuator elements.

8. Conclusions

In this paper, modal control of the thin shell structures is studied using discretely distributed piezoelectric elements. The quasi-modal sensor is designed to observe the main modal coordinates of the smart shell, and a simple criterion for finding the optimal location and sizes of the sensor elements is given so that the observation spillover can be minimized. Also, the quasi-modal actuator is developed to generate the designated modal control forces. Similarly, a criterion for optimizing the locations and sizes of the actuator

elements is also given in which both the energy and control spillover are considered. In addition, a compensator is used to each mode to perform the modal control of the smart shell independently which can further suppress the observation spillover. The simulation results show that the modal sensor can successfully provide modal signals used in the modal control of the shell although its basic frequency is high, provided that the proper amounts, locations and sizes of the sensor and actuators are used. As a result, the vibration of the shell can be suppressed effectively and the control voltages on the actuator elements are distributed in a balanced manner due to optimal placement of the actuator elements. The present method is suitable for vibration control of the large shell structures partially covered by the piezoelectric layers.

Acknowledgements

The authors are grateful to the funding by the Australian Research Council (No. A89905990) and by the National Science Foundation of China (No. 19802016).

References

Chandrashekhara, K., Smyser, C.P., Agrawal, S., 1998. Modeling and neural control of composite shells using piezoelectric devices. Journal of Intelligent Material Systems and Structures 9, 29–43.

Chee, C., Tong, L., Steven, G.P., 1998. A review on the modeling of piezoelectric sensors and actuators incorporated in intelligent structures. Journal of Intelligent Material Systems and Structures 9, 3–19.

Fanson, J.L., Caughey, T.K., 1990. Positive position feedback control for large space structures. AIAA Journal 28, 717–724.

Henry, J.K., Clark, R.L., 1999. A curved piezo-structures model: implications and active structural acoustic control. Journal of the Acoustical Society of America 106, 1400–1407.

Koconis, P.B., Kooler, L.P., Springer, G.S., 1994. Shape control of composite plates and shells with embedded actuators: ii desired shape specified. Journal of Composite Material 28, 262–285.

Lee, C.-K., Moon, F.C., 1990. Modal sensors and actuators. Journal of Applied Mechanics 57, 434–441.

Miller, S.E., Abramovich, H., 1996. A self-sensing piezoelectric actuator model for shells using first order shear deformation theory. Journal of Intelligent Materials and Structures 6, 624–638.

Pletner, B., Abramovich, H., 1997. Consistent methodology for the modeling of piezolaminated shells. AIAA Journal 35, 1316–1326.

Saravanos, D.A., 1996. Coupled mixed-filed laminate theory and finite element for smart piezoelectric composite shell structures. NASA CR 198490.

Sun, D.-C., Wang, D.J., Xu, Z.L., 1997. Distributed piezoelectric segment method for vibration control of smart beams. AIAA Journal 35, 583–584.

Sun, D.-C., Wang, D.J., Xu, Z.L., 1999a. Distributed piezoelectric element method for vibration control of smart plates. AIAA Journal 37, 1459–1463.

Sun, D.-C., Tong, L., Wang, D.-J., 1999b. Vibration control of smart plates using discretely distributed piezoelectric quasi-modal actuators/sensors, submitted for publication.

Thrupathi, S.R., Naganathan, N.G., 1993. A composite shell finite element for the analysis of smart structure. Proceedings of SPIE 1916, 424–437.

Tzou, H.-S., Gadre, M., 1989. Theoretical analysis of a multi-layered thin shell coupled with piezoelectric shell actuators for distributed vibration controls. Journal of Sound and Vibration 132, 433–450.

Tzou, H.-S., 1992. Active piezoelectric shell continua. In: Tzou, H.-S., Anderson G.L. (Eds.), Intelligent Structural Systems Kluwer, Dordrecht, pp. 9–74.

Tzou, H.-S., Zhong, J.P, Hollkamp, J.J., 1994. Spatially distributed orthogonal piezoelectric shell actuators: theory and applications. Journal of Sound and Vibration 174, 363–378.